RSC Advances

PAPER

View Article Online
View Journal | View Issue



Cite this: *RSC Adv.*, 2025, **15**, 50571

# Computational and experimental determination of electrochemical standard rate constant from cyclic voltammetry: insights into $\alpha + \beta \neq 1$ systems

Rania Saad Guermeche,[a] Abed Mohamed Affoune,*[a] Sabrina Houam,[a] Imene Atek,[b] Christine Vautrin-Ul,[c] Mouna Nacef,[a] Mohamed Lyamine Chelaghmia,[a] Hubert H. Girault,[d] Craig E. Banks[e] and Ilhem Djaghout[a]

In this work an in-depth examination of the soluble–soluble electrochemical system is presented, focusing on the challenge of accurately describing redox kinetics when the cathodic and anodic transfer coefficients do not necessarily sum to unity ($\alpha + \beta \neq 1$). A detailed approach that combines simulation calculations with experimental testing through cyclic voltammetry (CV) was employed. Kinetic curves with interpolation equations were established for the determination of the electrochemical standard heterogeneous rate constant ($k^0$). These kinetic curves illustrate the relationship between the difference in anodic and cathodic cyclic voltammetric peak potentials ($\Delta E_p$), the cathodic charge transfer coefficient ($\alpha$), and $k^0$. Interpolation equations were derived for both cases, when $\alpha + \beta = 1$ and when $\alpha + \beta \neq 1$, allowing a more comprehensive treatment of electron transfer kinetics, and additional kinetic curves were added. Experimental validation of these theoretical kinetic results was carried out by analyzing CVs for the electro-oxidation of ferrocyanide yielding a $k^0$ value of $(4.76 \pm 0.49) \times 10^{-6}$ m s$^{-1}$ with an average deviation between theoretical and experimental $\Delta E_p$ of $0.024 \pm 0.014$ V. The close alignment between the theoretical voltammograms and experimental results highlights the reliability of the model and marks a significant step forward in accurately characterizing electrochemical reaction kinetics.

Received 5th October 2025
Accepted 5th December 2025

DOI: 10.1039/d5ra07591b

rsc.li/rsc-advances



## 1 Introduction

Voltammetry is a widely utilized technique for investigating electrode processes and finds applications across diverse fields, including electrocatalytic studies, agroalimentary and health systems, and the analysis of biologically significant compounds. It is also employed in exploring the chemical composition of solid inorganic materials. In electrochemistry, voltammetry serves as a powerful tool for examining the thermodynamics and kinetics of electrode reactions. Among the various voltammetric techniques, cyclic voltammetry is the most commonly applied.[1]

The cyclic voltammetry (CV) simulation has been a focal point for numerous researchers.[1–22] Through the establishment of precise mathematical models and a profound understanding of system mechanisms, researchers attempt to solve the intricacies of CV curves.

The initiation of cyclic voltammetry simulation for one-step soluble–soluble redox systems traces its roots to the pioneering works of Randles and Ševčík[2,3] on reversible systems. This was later extended to quasi-reversible electron transfer by Matsuda and Ayabe in 1955,[4] followed by Nicholson in 1965[5] and recently by Houam.[6] Nicholson and Shain's work, has significantly contributed to this field.

The electrochemical standard heterogeneous rate constant ($k^0$) is a parameter of paramount significance as it serves as a clear indicator of the reaction's speed.[7,19,23–25] For this reason, numerous studies have focused on estimating $k^0$ for soluble–soluble redox couples in quasi-reversible and irreversible electrode reactions.[5,6,26–29] The calculation of $k^0$ is typically based either on single points of LSV curves corresponding to the peak or half-peak coordinates or on double points of CV corresponding to the anodic and cathodic peaks potentials. Concerning LSV, Matsuda[4] was the first to develop kinetic curves illustrating the variations of peak current, half-peak width, and peak potential as a function of the charge transfer coefficient ($\alpha$) and the standard

[a]*Laboratory of Industrial Analysis and Material Engineering, Department of Process Engineering, University 8 May 1945 Guelma, BP 401, Guelma 24000, Algeria. E-mail: affoune2@gmail.com*

[b]*Laboratory of Process Engineering for Sustainable Development and Health Products, Preparatory Classes Department, National Polytechnic School of Constantine, Constantine 25000, Algeria*

[c]*Laboratoire ICMN Interfaces, Confinement, Matériaux et Nanostructures, UMR7374, Université d'Orléans–CNRS, 1b Rue de la Férollerie, 45071, Orléans Cedex 2, France*

[d]*Laboratoire d'Electrochimie Physique et Analytique, École Polytechnique Fédérale de Lausanne, EPFL Valais Wallis, Rue de l'Industrie 17, Case Postale 440, CH-1951 Sion, Switzerland*

[e]*Faculty of Science and Engineering, Manchester Metropolitan University, Dalton Building, Chester Street, Manchester M1 5GD, UK*

heterogeneous rate constant for quasi-reversible soluble–soluble systems. Recently, Houam[6] have shown how to extract the $k^0$ through the development of interpolation equations based on peak current, half-peak width and peak potential kinetic curves.

Regarding cyclic voltammetry, the determination of $k^0$ from peak-to-peak potential separation ($\Delta E_p$) was first developed by Nicholson[5] in the form of a kinetic curve in the case where the charge transfer coefficient $\alpha = 0.5$. Lavagnini[26] later expanded on this by proposing a relationship between the dimensionless kinetic parameter and $\Delta E_p$, but only for cases where $\alpha = 0.5$ and $\Delta E_p \leq 200$ mV for soluble–soluble couples. Prior to this, Klingler[28] presented another equation as function of $\alpha$ and $\Delta E_p$ when $\alpha + \beta = 1$, Swaddle[29] as well, proposed an equation derived from Nicholson's $\Delta E_p$ results for $\alpha = 0.5$. To the best of our knowledge, no study has addressed the determination of the electrochemical standard kinetic rate constant for soluble–soluble systems over wide ranges of $\Delta E_p$ and $\alpha$, especially under conditions where $\alpha + \beta \neq 1$.

Voltammetry, particularly cyclic voltammetry (CV), remains a pivotal technique for probing electrode processes across a wide range of scientific and industrial applications. While the simulation of CV has garnered considerable research attention, the accurate determination of the electrochemical standard heterogeneous rate constant ($k^0$) continues to pose theoretical and practical challenges.

In this paper, we aim to thoroughly investigate the effects of $\alpha$, $\beta$, and their sum ($\alpha + \beta$) on cyclic voltammetry of soluble–soluble electrochemical system, with particular emphasis on their influence on peak-to-peak separation and the precise determination of the heterogeneous rate constant $k^0$. The calculation was performed using a semi-analytical computational approach. We looked into the fine points of the voltammograms, with a particular focus on the difference between the anodic and cathodic peak potentials ($\Delta E_p$). We developed kinetic curves showing the peak-to-peak potential separation as function of charge transfer coefficient and dimensionless rate constant. Interpolation equations were presented as a function of the dimensionless rate constant and charge transfer coefficient. The effect of the sum $\alpha + \beta$ on the calculation of $k^0$ was considered, and adjustments were made. Experimental investigation has been conducted to validate our theoretical results and pointed out the limitations of existing literature equations. The results obtained can be used to determine the electrochemical standard heterogeneous rate constant ($k^0$) for soluble–soluble redox systems from peak-to-peak potential separation of cyclic voltammograms.

## 2 Theory

The cyclic voltammetry computation was conducted using semi-analytical technique based on Nicholson's method. These calculations correspond to the reduction of a soluble oxidizing species (Ox) into a reducing species (Red), which is soluble. The reaction is represented by the equation below:

$$\mathrm{Ox} + n\acute{e} \Leftrightarrow \mathrm{Red} \tag{1}$$

The current changes following the Butler–Volmer equation:

$$I = nFAk^0\left[C_{\mathrm{Red}}(0,t)\exp\left(\frac{\beta nF\left(E-E^0\right)}{RT}\right) - C_{\mathrm{Ox}}(0,t)\exp\left(\frac{-\alpha nF\left(E-E^0\right)}{RT}\right)\right] \tag{2}$$

here, $\beta$ and $\alpha$ denote the anodic and cathodic charge transfer coefficients, respectively. Although the notation may differ across the literature,[5,17,30,31] the underlying physical meaning remains unchanged.

The definition of the parameters used in this equation can be found in Nomenclature section (see SI).

In this study, we examined both the case where $\alpha + \beta = 1$ and the case where $\alpha + \beta \neq 1$. Assuming that migration and convection in the electrolyte are negligible, Fick's second law is employed:

$$\frac{\partial C(x,t)}{\partial t} = D\frac{\partial^2 C(x,t)}{\partial x^2} \tag{3}$$

where: $x$: distance from the electrode; $t$: time; $C$: concentration of the electroactive species; $D$: diffusion coefficient.

The potential $E(t)$ for CV, is being swept depending on the relations:

$$0 < t \leq \lambda, \quad E(t) = E_i - vt \tag{4}$$

$$t > \lambda, \quad E(t) = E_i - 2v\lambda + vt \tag{5}$$

where: $E_i$: initial potential; $\lambda$: switching time.

The initial potential $E_i$ obeys the Nernst equation:

$$E_i = E_{eq} = E^0 + \frac{RT}{nF}\ln\left(\frac{C^*_{\mathrm{Ox}}}{C^*_{\mathrm{Red}}}\right) \tag{6}$$

Taking into consideration the following initial and boundary conditions, and assuming that, initially, only Ox species are present in the bulk solution:

$$t = 0, \quad x \geq 0, \quad C_{\mathrm{Ox}}(x,0) = C^*_{\mathrm{Ox}} \tag{7}$$

$$t > 0, \quad x \to \infty, \quad C_{\mathrm{Ox}}(\infty, t) = C^*_{\mathrm{Ox}} \tag{8}$$

$$t > 0, \quad x \to 0, \quad J_{\mathrm{Ox}}(0,t) = \frac{I(t)}{nFA} = -D_{\mathrm{Ox}}\left[\frac{\partial C_{\mathrm{Ox}}(x,t)}{\partial x}\right]_{x=0} \tag{9}$$

Fick's second law (3) is solved by applying the Laplace transform under the initial and boundary conditions (7), (8) and (9). The following expression related to the concentration of Ox species at the surface of electrode ($x = 0$) at any time ($t$), $C_{\mathrm{Ox}}(0,t)$, is obtained:

$$C_{\mathrm{Ox}}(0,t) = C^*_{\mathrm{Ox}} + \frac{1}{nFA\sqrt{\pi D_{\mathrm{Ox}}}}\int_0^t \frac{I(\tau)}{\sqrt{t-\tau}}\mathrm{d}\tau \tag{10}$$

Concerning the Red species, for the soluble–soluble systems:

$$C_{\mathrm{Red}}(0,t) = -\frac{1}{nFA\sqrt{D_{\mathrm{Red}}}}\frac{1}{\sqrt{\pi}}\int_0^t \frac{I(\tau)}{\sqrt{t-\tau}}\mathrm{d}\tau \tag{11}$$

By combination of the eqn (2), (4)–(6), (10) and (11), the expression of the current is given as follows:

$$I(t) = nFAC_{\mathrm{Ox}}^{*} {D_{\mathrm{Ox}}}^{1/2} \left(\frac{nF}{RT}\right)^{1/2} v^{1/2} \pi^{1/2} \chi(\sigma t) \tag{12}$$

where the dimensionless current $\chi(\sigma t)$, for soluble–soluble species, is given by the integral:

$$\int_0^{\sigma t} \frac{\chi(z)}{\sqrt{\sigma t - z}} \mathrm{d}z = \left[ - \frac{1}{\left[1 + [\theta S(\sigma t)]^{(\alpha+\beta)}\right]} \right] \left[1 + (\Lambda \chi(\sigma t))[\theta S(\sigma t)]^{\beta}\right] \tag{13}$$

For the soluble–soluble voltammograms, the dimensionless rate constant $\Lambda$ is the reversibility factor defined by Matsuda:[4]

$$\Lambda = \frac{k^0}{(\sigma D_{\mathrm{Ox}})^{1/2}} \tag{14}$$

where:

$$\sigma = \frac{nFv}{RT} \tag{15}$$

To make it easier to model, the dimensioned variables are transformed to dimensionless form, where:

$$S(\sigma t) = \exp(-\sigma t) \tag{16}$$

and where the initial potential is expressed as:

$$\mathrm{Init} = \frac{nF}{RT}\left(E_{\mathrm{i}} - E^0\right) \tag{17}$$

and the applied potential as:

$$\Phi = \frac{nF}{RT}\left(E(t) - E^0\right) = \mathrm{Init} - \sigma t \tag{18}$$

The numerical method developed by Nicholson[5] was used to calculate the integral (13), giving the following algorithms for the soluble–soluble system:

$$\chi(1)\sqrt{K} + \sum_{i=1}^{K-1} \sqrt{K - i}[\chi(i+1) - \chi(i)] = -\frac{1}{2\sqrt{\delta}} \left[\frac{1}{1 + [\theta S(\delta K)]^{(\alpha+\beta)}}\right] \left[1 + \left(\Lambda \chi(\delta K)[\theta S(\delta K)]^{\beta}\right)\right] \tag{19}$$

where ($\delta$) represents the calculation step.

Providing the values of the $\delta$, Init, $\Phi$, $\alpha$, $\beta$, $\Lambda$ in the corresponding algorithm, the dimensionless cyclic voltammograms can be computed.

# 3 Experimental

## 3.1 Calculation methods

Our simulations were implemented in Fortran 90 and compiled with Microsoft Fortran PowerStation 4.0. The resulting data was then processed and visualized using Origin 2018, which provided comprehensive tools for analysis. To estimate the charge transfer coefficient, Tafel analysis was applied. Additionally, the diffusion coefficient was determined *via* the semi-integration method, following the algorithm originally outlined by Oldham.[14,32,33]

## 3.2 Reagents

For the electrochemical oxidation reaction, we used potassium ferrocyanide, $K_4Fe(CN)_6$ (99%) (5 mM) in potassium chloride KCl (99%) (0.1 M). All reagents were used without purification and were purchased from Sigma-Aldrich Company.

## 3.3 Instrumentation and procedures

The cyclic voltammetric measurements were performed using a VersaSTAT 3 Potentiostat (Princeton Applied Research, AMETEK, USA).

Screen-printed graphite electrodes (SPEs) from Manchester Metropolitan University were used without any pre-treatment. The SPE comprised of a graphite working electrode (0.0707 $cm^2$), a graphite counter electrode, and an Ag/AgCl reference electrode. The experiments were carried out at room temperature.

# 4 Results and discussion

## 4.1 General features of voltammograms

Fig. 1 represents theoretical cyclic voltammograms for soluble–soluble redox systems, calculated with two values ($10^{-3}$ and $10^{3}$) of the dimensionless rate constant $\Lambda$, for $\alpha = 0.5$. $\Lambda$ is linked to the electrochemical rate constant ($k^0$) by the eqn (14) ($\Lambda = k^0/\sqrt{nFvD_{\mathrm{Ox}}/RT}$). The Fig. 2 illustrates the influence of the cathodic charge transfer coefficient ($\alpha$) on the cyclic voltammograms. The simulations were conducted using the following parameters: $n = 1$, $T = 298.15$ K, $v = 0.1$ V $s^{-1}$, $D = 1 \times 10^{-9}$ $m^2$ $s^{-1}$, $C_{\mathrm{Ox}}^{*} = 1$ mM, $A = 1$ $cm^2$.

Fig. 1 shows that the cathodic peaks exhibit an asymmetric convex shape. The peak arises from the transition between a charge transfer-controlled regime (with an exponential function between current and time) and a diffusion-controlled regime (with an inversely proportional function between current and time). Upon reversing the potential scan direction, the cathodic current continues to decrease, and after reaching zero, it follows an exponential rise.

In Fig. 1 (right), irreversibility, when $\Lambda = 10^{-3}$, results in a separation between the anodic and cathodic peak potentials ($\Delta E_{\mathrm{p}}$). This separation increases with higher irreversibility (*i.e.*, with decreasing rate constant $\Lambda$) and with a lower cathodic charge transfer coefficient ($\alpha$). Nicholson and other authors[5,26,28,29] have analyzed the influence of the rate constant on $\Delta E_{\mathrm{p}}$ for $\alpha = 0.5$ in soluble–soluble redox systems, considering limited values of $\Lambda$. In this work, we extend this analysis, by investigating the effect of the rate constant on $\Delta E_{\mathrm{p}}$ over the ranges of $\alpha = [0.1\text{–}0.9]$ and $\Lambda = [10^{-6}$ to $10^{6}]$.

The rate at which the cathodic peak is reached decreases as irreversibility increases and the cathodic charge transfer coefficient diminishes, as shown in Fig. 2.

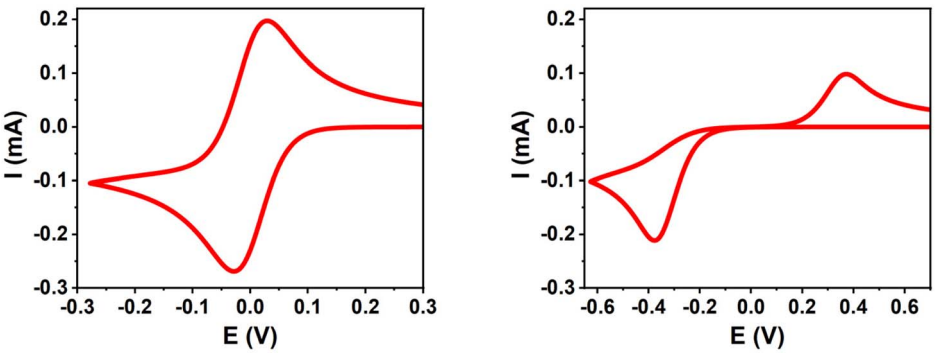


Fig. 1 Presentation of soluble–soluble voltammograms for: $\Lambda = 10^3$ (left) and $\Lambda = 10^{-3}$ (right).

### 4.2 Effect of switching potential $E_\lambda$

To assess the effect of the switching potential on $\Delta E_p$, five values were selected: 0 V, −0.1 V, −0.2 V, −0.25 V and −0.3 V *versus* the cathodic peak potential, as shown in Table 1. Calculations were performed for soluble–soluble redox systems under reversible, quasi-reversible and irreversible conditions. The cathodic transfer coefficient was set to 0.3, 0.5 and 0.7, considering the condition $\alpha + \beta = 1$. We notice that for reversible system cathodic transfer coefficient has no effect on $\Delta E_p$.

The results in Table 1 show that when $E_\lambda < -0.1$ V relative to the cathodic peak potential $E_{pc}$, the effect of $E_\lambda$ on $\Delta E_p$ is negligible, regardless of reversibility. These observations related to the effect of the switching potential remain valid even when $\alpha + \beta \neq 1$.

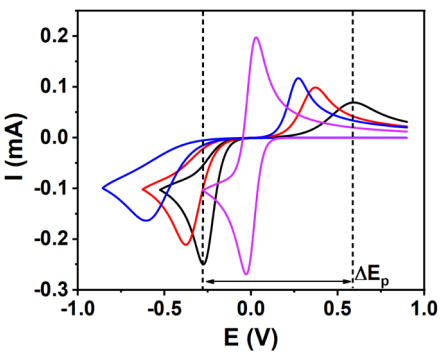


Fig. 2 Charge transfer coefficient effect on soluble–soluble voltammograms: $\alpha = 0.7$ (black), $\alpha = 0.5$ (red), $\alpha = 0.3$ (blue) for $\Lambda = 10^{-3}$ and $\alpha = 0.5$ (magenta) for $\Lambda = 10^3$.

Given that the sum of $\alpha + \beta$ influences the peak potentials and, consequently, the $\Delta E_p$ values, the following study explores its effect in detail. We analyze the cases where $\alpha + \beta = 1$ and $\alpha + \beta \neq 1$ separately.

### 4.3 Determination of the standard heterogeneous rate constant ($k^0$) for the case where $\alpha + \beta = 1$

In order to evaluate the standard heterogeneous rate constant ($k^0$), we investigate the combined effect of cathodic charge transfer coefficient and dimensionless rate constant on $\Delta E_p$.

The relationship between dimensional ($\Delta E_p$) and dimensionless ($\Delta\Phi$) peak-to-peak potential separations is as follows:

$$\Delta\Phi = \left(\frac{nF}{RT}\right) \times \Delta E_p \tag{20}$$

In the literature, Nicholson was the first to investigate the effect of the dimensionless kinetic parameter $\Psi$ ($\Psi = \Lambda\pi^{-1/2}$) on $n\Delta E_p$ at $\alpha = 0.5$. Based on his diagram,[5] an empirical equation was afterwards established by Lavagnini[26] which is valid for $0.1 \leq \Lambda\pi^{-1/2} \leq 7$ and for $n\Delta E_p$ values up to 200 mV:

$$k^0 = \frac{(-0.6288 + 0.0021 n\Delta E_p)}{(1 - 0.017 n\Delta E_p)} \sqrt{\frac{\pi D n v F}{RT}} \tag{21}$$

On the other hand, Klingler[28] proposed an equation that considers the effect of the charge transfer coefficient ($\alpha$):

$$k^0 = 2.18\sqrt{\frac{\alpha D n v F}{RT}} \exp\left(-\frac{\alpha^2 n F \Delta E_p}{RT}\right) \tag{22}$$

Table 1 $\Delta E_p$ as function of $\Lambda$, $\alpha$ and $E_\lambda$

| | | | $\Delta E_p$, V | | | | |
|---|---|---|---|---|---|---|---|
| | | | $E_\lambda$ *vs.* $E_{pc}$ | $E_\lambda$ *vs.* $E_{pc}$ | $E_\lambda$ *vs.* $E_{pc}$ | $E_\lambda$ *vs.* $E_{pc}$ | $E_\lambda$ *vs.* $E_{pc}$ |
| Reversibility | $\Lambda$ | $\alpha$ | −0 V | −0.1 V | −0.2 V | −0.25 V | −0.3 V |
| Reversible | $10^3$ | — | 0.069 | 0.058 | 0.058 | 0.058 | 0.058 |
| Quasi- reversible | $10^0$ | 0.3 | 0.104 | 0.099 | 0.099 | 0.099 | 0.099 |
| | | 0.5 | 0.104 | 0.099 | 0.099 | 0.099 | 0.099 |
| | | 0.7 | 0.102 | 0.096 | 0.096 | 0.095 | 0.096 |
| Irreversible | $10^{-3}$ | 0.3 | 0.879 | 0.880 | 0.880 | 0.880 | 0.880 |
| | | 0.5 | 0.747 | 0.748 | 0.748 | 0.748 | 0.749 |
| | | 0.7 | 0.865 | 0.867 | 0.868 | 0.869 | 0.870 |

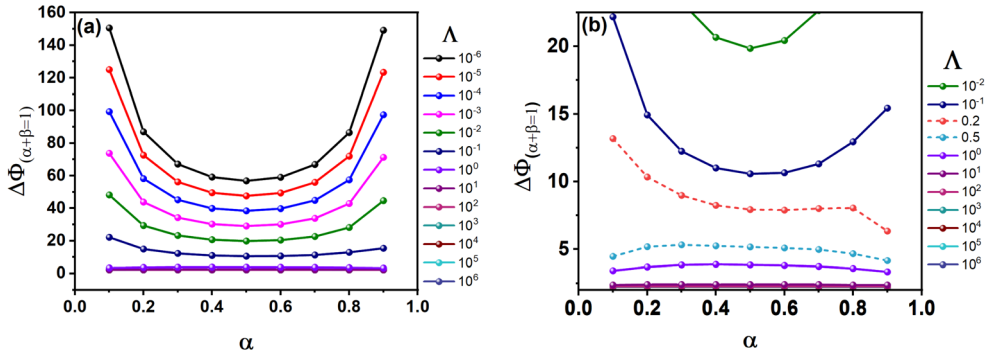


Fig. 3 Presentation of the effect of the charge transfer coefficient ($\alpha$) and the kinetic rate constants $\Lambda$ on the peak-to-peak potential separation $\Delta\Phi$: (a) ($10^{-6} \leq \Lambda \leq 10^{6}$), (b) $\Lambda \geq 10^{-2}$.

Later, Swaddle,[29] presented another equation based on Nicholson's $\Delta E_p$ values:

$$\mathrm{Ln}\,\Psi = 3.69 - 1.16\ln(\Delta E_p - 59) \quad (23)$$

In our work, we will explore a larger interval of ($\Lambda$) from $10^{-6}$ to $10^{6}$ and ($\alpha$) from 0.1 to 0.9.

Fig. 3 displays kinetic curves illustrating how the dimensionless peak-to-peak potential separation ($\Delta\Phi$) changes as a function of $\alpha$ and the logarithm of the dimensionless rate constant $\log(\Lambda)$ for soluble–soluble redox systems. We denote the peak-to-peak potential separation $\Delta\Phi_{(\alpha+\beta=1)}$ for soluble–soluble systems, when necessary. Fig. 3a shows a symmetrical convex shape centered at $\alpha = 0.5$ for $\Lambda$ values in the range $10^{-6}$ to $10^{-1}$. As $\Lambda$ increases above $10^{-1}$, the curves become increasingly asymmetrical and flattened, particularly from $\Lambda = 10$ onward to $10^{6}$, as shown in Fig. 3b.

These kinetic curves can be used to determine $\Lambda$ when the values of $\alpha$ and $\Delta E_p$ are known. Once $\Lambda$ is obtained, the standard rate constant $k^0$ can be calculated using eqn (14). The diagrams were constructed from cyclic voltammograms, starting in the cathodic direction of potential, with the cathodic transfer coefficient denoted as ($\alpha$). In the initial state, only the oxidized species are present, without the reduced species. In the case of an anodic start of potential, with presence of only reduced species in the initial state, the anodic transfer coefficient denoted as ($\beta$). The same diagram remains valid by replacing $\alpha$ with $\beta$.

Symmetry allows that interpolation is feasible within the ranges when $\Lambda \leq 10^{-1}$. The data interpolation was carried out using the rational Holliday equation, fitted within the following parameter ranges: $0.1 \leq \alpha \leq 0.9$, $-6 \leq \log(\Lambda) \leq -1$, $10 \leq \Delta\Phi \leq 150$:

$$y = \frac{1}{a + bx + cx^2} \quad (24)$$

where $y$ represents $\Delta\Phi$ and $x$ represents $\alpha$. $a$, $b$ and $c$ are functions of $\log(\Lambda)$.

The following equation was obtained:

$$\Delta\Phi_{(\alpha+\beta=1)} = \frac{1}{a + b\alpha + c\alpha^2};\ R_2 = 0.9999 \quad (25)$$

where:

$$a = 7.50978 \times 10^{-4} + 0.10944\exp(1.72596\log(\Lambda));\ R^2 = 0.9994 \quad (26)$$

$$b = 0.05374 + 0.37723\exp(0.52667\log(\Lambda));\ R^2 = 0.9994 \quad (27)$$

$$c = -0.04452 - 0.32511\exp(0.43694\log(\Lambda));\ R^2 = 0.9994 \quad (28)$$

When the sum of $\alpha + \beta = 1$ and $\Lambda \leq 10^{-1}$, either the kinetic curves in Fig. 3 or the interpolation eqn (25) can be used to directly determine $\Lambda$. For $\Lambda > 10^{-1}$, interpolation cannot be performed due to the irregular shape of the kinetic curves in these ranges; However, $\Lambda$ can still be estimated from the zoomed curves in Fig. 3b, where $\alpha$ has a minor effect on $\Delta\Phi$.

### 4.4 Determination of the standard heterogeneous rate constant ($k^0$) for the case where $\alpha + \beta \neq 1$

Electrochemical literature reports that the sum of the charge transfer coefficients, $\alpha + \beta$, can be either less than or greater than one. As noted by Chen[34] in Butler–Volmer theory, $\alpha + \beta = 1$ is assumed from microscopic reversibility but strictly holds only at the equilibrium potential; in quasi-reversible systems this condition breaks down, and Marcus–Hush theory (especially its asymmetric form) explains deviations by relating them to differences in vibrational force constants of the redox species. In this context, $\alpha$ and $\beta$ may be viewed as empirical parameters reflecting the relative slopes of the oxidized and reduced potential energy surfaces, where $\alpha + \beta \neq 1$ indicates asymmetric

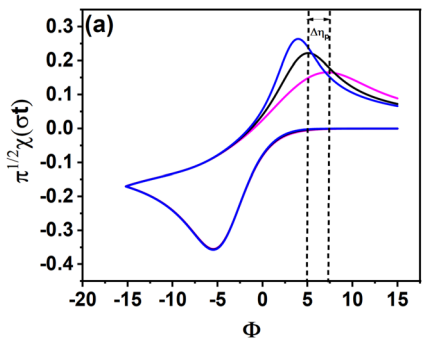


Fig. 4 Dimensionless cyclic voltammograms for $\Lambda = 10^{-1}$, $\alpha = 0.5$ and $\beta = 0.3, 0.5, 0.7$.

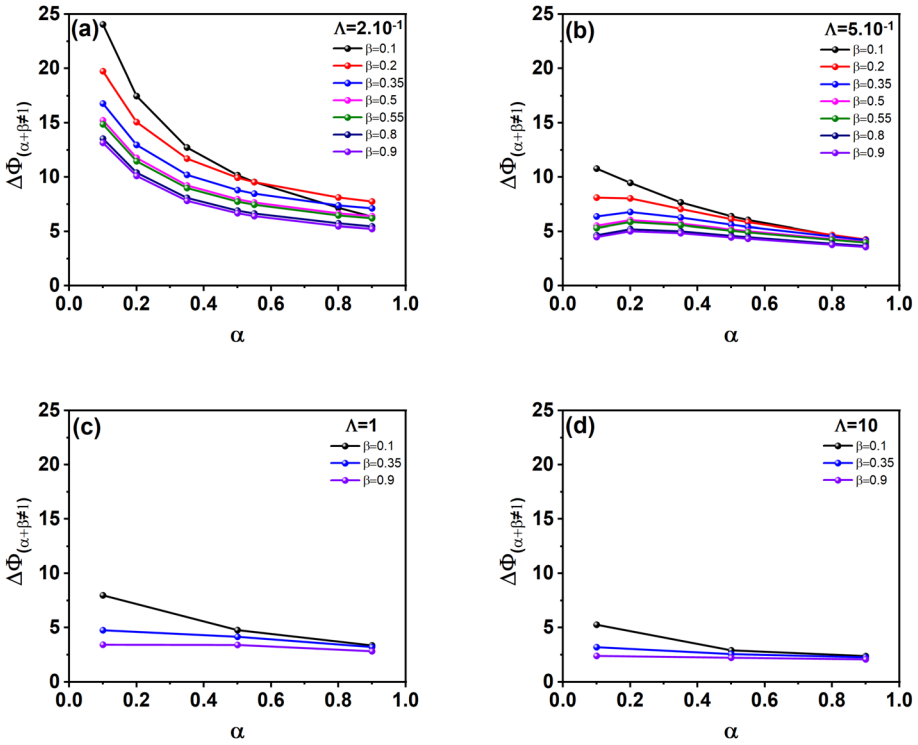


Fig. 5 Effect of the cathodic ($\alpha$) and anodic ($\beta$) charge transfer coefficients where $\alpha + \beta \neq 1$ and the kinetic rate constant $\Lambda$, on the peak-to-peak potential separation $\Delta\Phi$ for: (a) $\Delta\Phi_{(\alpha+\beta\neq1)}$ for $\Lambda = 2 \times 10^{-1}$, (b) $\Delta\Phi_{(\alpha+\beta\neq1)}$ for $\Lambda = 5 \times 10^{-1}$, (c) $\Delta\Phi_{(\alpha+\beta\neq1)}$ for $\Lambda = 1$, (d) $\Delta\Phi_{(\alpha+\beta\neq1)}$ for $\Lambda = 10$.

surfaces and unequal reorganization energies ($\lambda$), thus linking the Butler–Volmer coefficients to measurable Marcus-Hush quantities.[35,36] Henstridge[37] reported that, due to the large peak-to-peak separation, the sum $\alpha + \beta = 1$ might be relaxed without violating the principle of microscopic reversibility, because the oxidation and reduction processes occur at very different potentials and, therefore, in different environments.

Different authors[38–43] reported experimental systems where $\alpha + \beta \neq 1$. Within a Butler–Volmer analysis, Suwatchara[44] demonstrated that assuming $\alpha + \beta = 1$ gave a poor description of the experimental CVs for the one-electron reduction of 2-nitropropane, whereas relaxing this constraint, $\alpha + \beta \neq 1$, yielded an excellent fit.

In Fig. 4, we present the effect of $\alpha + \beta \neq 1$ on the anodic peak, where $\alpha$ fixed at 0.5 and $\beta$ set to 0.3, 0.5 or 0.7. The figure shows a difference between the dimensionless anodic peak potentials for $\alpha + \beta \neq 1$ and $\alpha + \beta = 1$, defined as:

$$\Delta\eta_p = \eta_{pa(\alpha+\beta\neq1)} - \eta_{pa(\alpha+\beta=1)} \quad (29)$$

With:

$$\eta_{pa} = \frac{nF}{RT}\left(E_p - E^0\right) \quad (30)$$

We observe that when the sum $\alpha + \beta \neq 1$, the dimensionless peak-to-peak difference $\Delta\Phi_{(\alpha+\beta\neq1)}$, is more adequate:

$$\Delta\Phi_{(\alpha+\beta\neq1)} = \Delta\Phi_{(\alpha+\beta=1)} + \Delta\eta_p \quad (31)$$

$\Delta\Phi_{(\alpha+\beta\neq1)}$ can be using obtained experimentally *via* eqn (20).

The corresponding $\Lambda$ value can be estimated using Fig. 5, or Table S1 (SI), based on $\alpha$, $\beta$, and $\Delta\Phi_{(\alpha+\beta\neq1)}$.

The association of $\Delta\eta_p$ with eqn (25), which is valid for $\log(\Lambda) \leq -1$, leads to new interpolation equation for $\Delta\Phi_{(\alpha+\beta\neq1)}$.

**4.4.1 Interpolation equation for the dimensionless peak-to-peak difference $\Delta\Phi_{(\alpha+\beta\neq1)}$: $\log(\Lambda) \leq -1$.** The LSV equation number (32) obtained by Houam *et al.*[6] for $\eta_p$ when $\log(\Lambda) \leq -1$ is used to express $\Delta\eta_p$ as a function of $\alpha$, $\beta$ and $\log(\Lambda)$:

$$\begin{aligned}\Delta\eta_p = {} & [(1.222 - 0.189\beta^{-1}) + (-2.296\beta^{-1})\log(\Lambda)] \\ & - [(1.222 - 0.189(1-\alpha)^{-1}) \\ & + (-2.296(1-\alpha)^{-1})\log(\Lambda)]\end{aligned} \quad (32)$$

By substituting eqn (32) and (25) into eqn (31), this latter becomes:

$$\Delta\Phi_{(\alpha+\beta\neq1)} = \Delta\Phi_{(\alpha+\beta=1)} + \Delta\eta_p \quad (33)$$

$$\begin{aligned}\Delta\Phi_{(\alpha+\beta\neq1)} = {} & \frac{1}{a + b\alpha + c\alpha^2} + \left[\left(1.222 - 0.189\beta^{-1}\right)\right. \\ & \left. + \left(-2.296\beta^{-1}\right)\log(\Lambda)\right] - \left[\left(1.222 - 0.189(1-\alpha)^{-1}\right)\right. \\ & \left. + \left(-2.296(1-\alpha)^{-1}\right)\log(\Lambda)\right]\end{aligned} \quad (34)$$

**4.4.2 Kinetic curves for $\alpha + \beta \neq 1$ and when Log($\Lambda$)> −1.** For $\log(\Lambda) > -1$, $\Delta\Phi$ becomes more sensitive to the individual values of $\alpha$ and $\beta$, and no universal interpolation equation can

Table 2 Standard heterogeneous rate constant ($k^0$) values for the oxidation of ferrocyanide ions

| $k^0$ calculation methods | $k^0$, $10^{-6}$ m s$^{-1}$ | $\Lambda$ |
|---|---|---|
| Kinetic curves where $\alpha + \beta = 1$ for soluble–soluble systems | 2.87 | 0.08 |
| Kinetic curves where $\alpha + \beta \neq 1$ for soluble–soluble systems | ≈7.09 | ≈0.20 |
| Interpolation equation where $\alpha + \beta = 1$ for soluble–soluble systems (25) | 2.74 | 0.08 |
| Interpolation equation where $\alpha + \beta \neq 1$ for soluble–soluble systems (34) | 5.90 | 0.17 |
| Lavagnini's equation where $\alpha + \beta = 1$ (21) | −1.83 | −0.05 |
| Klingler's equation where $\alpha + \beta = 1$ (22) | 14.82 | 0.42 |
| Swaddle's equation where $\alpha + \beta = 1$ (23) | 3.23 | 0.09 |
| LSV method (ferrocyanide electro-oxidation)[6] | 5.19 | — |
| CV method (ferricyanide electro-reduction)[45] | 4.01 | — |
| EIS method (ferrocyanide electro-oxidation)[46] | $11 \times 10^4$ | — |
| EIS method (ferro/ferricyanide)[45] | 0.22 | — |

be established. Therefore, $\Lambda$ is determined directly from the kinetic curves shown in Fig. 5, for $\Delta\Phi < 25$, given $\alpha$, $\beta$, and $\Delta E_p$.

### 4.5 Theoretical validation of interpolation equations

To validate our interpolation equations, we performed calculations for a large number of cyclic voltammograms using different values of $\alpha$, $\beta$, $\alpha + \beta$, and $\Lambda$. For each voltammogram, we first determined the peak-to-peak separation. We then calculated the corresponding dimensionless kinetic parameter ($\Lambda'$) using all the interpolation equations. The calculated $\Lambda'$ values showed close agreement with the input $\Lambda$, as summarized in Table S1. Small differences arise only from numerical precision during calculation using MATLAB software (see SI).

Analysis of the results in Table S1 led to the following conclusions:

• The results confirm that the proposed interpolation equations are valid over a wide range of kinetic regimes, whether $\alpha + \beta = 1$ or $\alpha + \beta \neq 1$.

• We have demonstrated the crucial role of the sum of $\alpha + \beta$ in determining $k^0$. Assuming $\alpha + \beta = 1$ or $\alpha = \beta = 0.5$ can lead to significant errors in the calculation of $k^0$, especially for irreversible systems.

• Additionally, when $\alpha$ or $\beta$ are very small (<0.2) or very large (>0.8), or when their sum ($\alpha + \beta$) is very low (<0.3) or very high (>1.2), $k^0$ determination becomes highly sensitive, and interpolation becomes necessary.

• As far as we know, the study offers detailed and consistent insights into the effects of $\alpha$, $\beta$, and $\alpha + \beta$ on cyclic voltammetry, particularly on peak-to-peak separation and their impact on the determination of $k^0$.

### 4.6 Experimental validation: case of ferrocyanide ions electro-oxidation

**4.6.1 Study at scan rate $\nu = 50$ mV s$^{-1}$.** Fig. S1 displays the experimental cyclic voltammogram related to the oxidation of ferrocyanide at screen-printed electrodes (SPEs) in a KCl electrolyte at a scan rate of $\nu = 50$ mV s$^{-1}$.

The reaction of this soluble–soluble redox system is as follows:

$$Fe(CN)_6^{4-} \rightleftharpoons Fe(CN)_6^{3-} + e^- \quad (35)$$

In order to calculate $k^0$, we need the anodic and cathodic charge transfer coefficients and the diffusion coefficient values (see SI). Tafel plots and the semi-integration technique (Fig. S1), were used to calculate charge transfer coefficients and the diffusion coefficient ($\alpha = 0.289 \pm 0.005$, $\beta = 0.259 \pm 0.003$, $D = 6.45 \times 10^{-10}$ m$^2$ s$^{-1}$) respectively. Regarding the calculation of $k^0$, we will use both kinetic curves and interpolation equations developed above.

In the experimental cyclic voltammogram shown in Fig. S1, the anodic peak potential is $38.28 \times 10^{-2}$ V and the cathodic peak potential is $0.92 \times 10^{-2}$ V, resulting in a peak-to-peak separation ($\Delta E_p = E_{pa} - E_{pc}$) of 0.37 V. According to the relationship (20), we obtain the following value of the dimensionless peak-to-peak separation $\Delta\Phi$ of ferro/ferricyanide oxidation–reduction:

$$\Delta\Phi = \left(\frac{nF}{RT}\right)\Delta E_p = 38.924 \times 0.37 = 14.54 \quad (36)$$

Standard heterogeneous rate constant ($k^0$) values for the oxidation of ferrocyanide ions, obtained from different kinetic curves and calculated from different equations are obtained in Table 2.

By applying the rule of three, based on the kinetic curves in Fig. 3a, where $\alpha + \beta = 1$, we can estimate the value of $\Lambda$ as follows: $\Lambda = (5.5\text{ cm} \times 0.09)/6.1\text{ cm} = 0.08$. Alternatively, by using the kinetic curves in Fig. 5 where $\alpha + \beta \neq 1$, the corresponding value of $\Lambda$ is approximatively equal to $2 \times 10^{-1}$ (Fig. 5a). Knowing the values of $\Lambda$ and $\beta$, the values of $k^0$ can be calculated using eqn (14) and are equal to $2.87 \times 10^{-6}$ m s$^{-1}$ ($\Lambda = 0.08$) and $k^0 = 7.09 \times 10^{-6}$ m s$^{-1}$ ($\Lambda = 0.20$). The interpolation eqn (25) where ($\alpha + \beta = 1$) and (34) ($\alpha + \beta \neq 1$), give the values of $k^0 = 2.74 \times 10^{-6}$ m s$^{-1}$ and $k^0 = 5.90 \times 10^{-6}$ m s$^{-1}$, respectively.

The calculation methods for $k^0$ using equations from other authors[26,28,29] were examined, and the obtained values are presented in Table 2. Lavagnini equation[26] has given negative value of $k^0 = -1.83 \times 10^{-6}$ m s$^{-1}$. While Klinger[28] method gave a standard rate constant value of $k^0 = 14.82 \times 10^{-6}$ m s$^{-1}$, the Swaddle equation led to a value of $k^0 = 3.23 \times 10^{-6}$ m s$^{-1}$. The negative value obtained from the Lavagnini equation arises because it is valid only for $\alpha = 0.5$ and $n\Delta E_p \leq 200$ mV. Klinger's reported value is roughly two to three times higher than our calculated value; this can be attributed to the fact that Klinger's

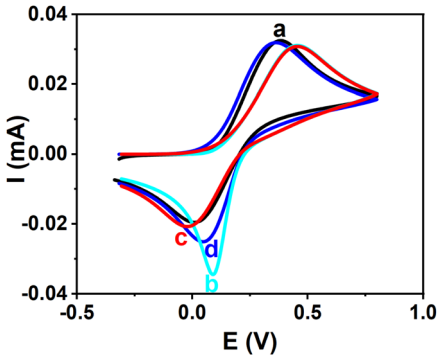


Fig. 6 Comparison between experimental CV of ferrocyanide redox reaction (a) black solid line, and simulated voltammograms where $k^0$ are calculated from kinetic curves: (b) $k^0 = 2.87 \times 10^{-6}$ m s$^{-1}$, $\beta = 0.259$, $\alpha = 0.741$ ($\alpha + \beta = 1$), cyan solid line (c) $k^0 = 2.87 \times 10^{-6}$ m s$^{-1}$ $\beta = 0.259$, $\alpha = 0.289$ ($\alpha + \beta \neq 1$) red solid line (d) $k^0 = 7.09 \times 10^{-6}$ m s$^{-1}$ $\beta = 0.259$, $\alpha = 0.289$ ($\alpha + \beta \neq 1$) blue solid line.

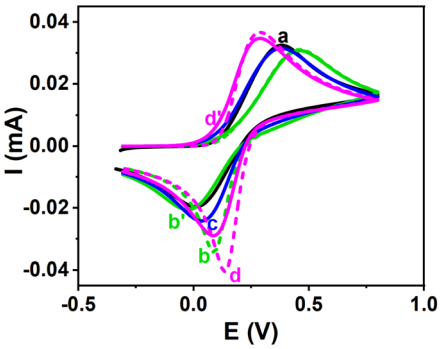


Fig. 7 Comparison between experimental CV of ferrocyanide redox reaction (a) black solid line and different theoretical curves where $k^0$ is calculated using interpolation equations: From eqn (25) (b) green dashed line: $k^0 = 2.74 \times 10^{-6}$ m s$^{-1}$, $\beta = 0.259$, $\alpha = 0.741$ ($\alpha + \beta = 1$). From eqn (25) (b′) green solid line: $k^0 = 2.74 \times 10^{-6}$ m s$^{-1}$, $\beta = 0.259$, $\alpha = 0.289$ ($\alpha + \beta \neq 1$). From eqn (34) (c) blue solid line: $k^0 = 5.90 \times 10^{-6}$ m s$^{-1}$, $\beta = 0.259$, $\alpha = 0.289$ ($\alpha + \beta \neq 1$). From Klingler's eqn (22) (d) magenta dashed line: $k^0 = 14.82 \times 10^{-6}$ m s$^{-1}$, $\beta = 0.259$, $\alpha = 0.741$ ($\alpha + \beta = 1$). From Klingler's eqn (22) (d′) magenta solid line: $k^0 = 14.82 \times 10^{-6}$ m s$^{-1}$, $\beta = 0.259$, $\alpha = 0.289$ ($\alpha + \beta \neq 1$).

equation applies only when the sum of $\alpha + \beta$ equals 1, whereas for the ferrocyanide redox reaction, the sum is 0.548. The $k^0$ value obtained from the Swaddle[29] equation is very close to that obtained using the interpolation eqn (25) where $\alpha + \beta = 1$. However, theoretical validation calculation (see SI; Table S2) show that the dimensionless rate constant values obtained using Swaddle's equation are high, and sometimes significantly higher, than the expected values, when the peak to peak potential separation increases or when the sum of $\alpha + \beta$ is low.

In what follows we will present the simulation of the cyclic voltammetric curves for the different calculated $k^0$ values.

Fig. 6 and 7 display both the simulated curves and the experimental cyclic voltammograms. The previously determined values of $\beta$, $D$, $k^0$ were used to simulate the cyclic voltammograms. For $\alpha$, we used either the value obtained from the Tafel plot or that calculated using the relation $\alpha = 1 - \beta$. Fig. 6 illustrates the comparison between the experimental curve and the simulated ones calculated using $k^0$ values deduced from kinetic curves. However, Fig. 7 presents the comparison when the simulated voltammograms were obtained using $k^0$ values calculated from interpolation equations.

It can be observed in Fig. 6 that the voltammogram in Fig. 6b, calculated using a $k^0$ value of $k^0 = 2.87 \times 10^{-6}$ m s$^{-1}$ obtained from the kinetic curves $\alpha + \beta = 1$ with $\beta = 0.259$ and $\alpha = 1 - \beta = 0.741$, does not fully overlay with the experimental CV in Fig. 6a, especially at the cathodic peak. Whereas, the calculated voltammogram in Fig. 6c using the same $k^0$ and $\beta$ values but with $\alpha$ equal to the value obtained from the Tafel plot (0.289), closely matches the experimental CV which indicates that we should use this latter rather than $\alpha = 1 - \beta$. With $k^0$ value of $k^0 = 7.09 \times 10^{-6}$ m s$^{-1}$ obtained from the kinetic curves $\alpha + \beta \neq 1$, the simulated voltammograms in Fig. 6b matches better than all other curves.

Using the value of $k^0 = 2.74 \times 10^{-6}$ m s$^{-1}$ obtained from the interpolation equation with $\alpha + \beta = 1$ (25), the resulting curve in Fig. 7b does not fully overlay with the experimental CV. However, when $\alpha + \beta \neq 1$, the simulated voltammogram (Fig. 7b′) is very close to the experimental curve. It is noted that the Fig. 7b overlaps with the curve calculated using $k^0 = 3.23 \times 10^{-6}$ m s$^{-1}$, obtained from the Swaddle equation, for this reason it was not included in Fig. 7. Furthermore, the simulation curves show that our $k^0$ values are more precise than that obtained by Klingler equation[28] and which used to calculate curves in Fig. 7d and d′ for $\alpha + \beta = 1$ and $\alpha + \beta \neq 1$, respectively. Moreover, when using the value of $k^0 = 5.90 \times 10^{-6}$ m s$^{-1}$ obtained from the interpolation eqn (34) where $\alpha + \beta \neq 1$, the obtained curve in Fig. 7c best matches the experimental curve (Fig. 7a). Recently, Houam[6] reported a value of $k^0 = 5.19 \times 10^{-6}$ m s$^{-1}$ based on linear sweep voltammetry (LSV) simulation using (eqn (27)), which is nearly identical to the value obtained in our study. Furthermore, a value of $k^0 = 4.01 \times 10^{-6}$ m s$^{-1}$ was reported on the electro-reduction of ferricyanide in PBS on SPE using CV technique.[45]

We also attempted to compare our cyclic voltammetry results with electrochemical impedance spectroscopy (EIS) data. However, we could not find results under the same experimental conditions used in this manuscript. The reported values corresponding to ferrocyanide electro-oxidation in KF on gold

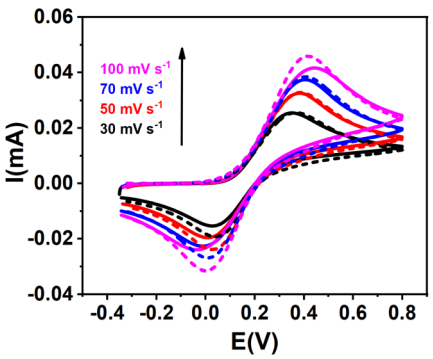


Fig. 8 Experimental (solid lines) and simulated (dashed lines) CVs for $[Fe(CN)_6]^{4-}/[Fe(CN)_6]^{3-}$, calculated with $\beta$, $\alpha$, $D$, $k^0$ mean values.

Table 3 Kinetic parameters values for $[Fe(CN)_6]^{4-}/[Fe(CN)_6]^{3-}$ (ferro/ferricyanide) redox couple at various scan rates; $k^0$ obtained from eqn (34)

| Scan rate mV $s^{-1}$ | $\beta$ | $\beta$ mean | $\alpha$ | $\alpha$ mean | $D$, $10^{-10}$ $m^2$ $s^{-1}$ | $D$, $10^{-10}$ $m^2$ $s^{-1}$ mean | $\Delta E_p$ V | $\Delta\Phi$ | $\Lambda$ | $k^0$, $10^{-6}$ m $s^{-1}$ | $k^0$ mean $10^{-6}$ m $s^{-1}$ |
|---|---|---|---|---|---|---|---|---|---|---|---|
| 30 | 0.307 ± 0.003 | 0.286 ± 0.015 | 0.265 ± 0.005 | 0.300 ± 0.016 | 6.85 | 6.43 ± 0.15 | 0.32 | 12.46 | 0.21 | 5.72 | 4.76 ± 0.49 |
| 50 | 0.259 ± 0.003 | | 0.289 ± 0.005 | | 6.45 | | 0.37 | 14.54 | 0.15 | 5.27 | |
| 70 | 0.259 ± 0.003 | | 0.305 ± 0.005 | | 6.27 | | 0.41 | 15.96 | 0.11 | 4.58 | |
| 100 | 0.317 ± 0.003 | | 0.340 ± 0.005 | | 6.16 | | 0.48 | 18.68 | 0.07 | 3.48 | |

electrode was $k^0 = 11 \times 10^{-2}$ m $s^{-1}$ [46], and in PBS on SPE was $k^0 = 0.22 \times 10^{-6}$ m $s^{-1}$ [45], differ markedly from our value on SPE electrodes ($k^0 = 5.90 \times 10^{-6}$ m $s^{-1}$). A significant difference can be observed between the values obtained from impedance measurements. Moreover, the electrode material and the electrolyte composition appear to have a strong influence on the reversibility of the redox couple.

These simulation results clearly indicate the importance of using the values of $\beta$ and $\alpha$ both obtained from the Tafel plots; determining one transfer coefficient from Tafel plots and then calculating the other using the equation $\alpha = 1 - \beta$ is not always appropriate.[44] Consequently, the interpolation equation with $\alpha + \beta \neq 1$ is more relevant.

**4.6.2 Scan rate effect.** The CVs at different scan rates are presented with calculation of their $\alpha$, $\beta$, $D$ and $k^0$ mean values. The same analysis carried out in Sub-sections 6.4.1 has been applied for all voltammograms using eqn (34) and the results are presented in Fig. 8 and Table 3.

The good agreement between simulated and experimental curves indicates that the standard rate constants determined in this work are reasonably accurate. The main discrepancies observed with ferrocyanide, mainly due to uncertainties in $k^0$ which is $(4.76 \pm 0.49) \times 10^{-6}$ m $s^{-1}$, which become more pronounced at high scan rates.

Since $k^0$ is an intrinsic property of a redox couple, it should ideally remain constant and independent of scan rate. However, Table 3 reveals a slight dependence on scan rate, which can likely be attributed to ohmic drop as well as to small uncertainties in the anodic and cathodic charge transfer coefficients and in the diffusion coefficient. The mean value of $k^0$ for ferrocyanide, with an error of $\pm 0.49 \times 10^{-6}$ m $s^{-1}$ (Table 3), suggests that the calculation remains reasonably reliable. The distortions observed at scan rate of 0.1 result from errors in the mean $k^0$, but this effect diminishes when the value $3.48 \times 10^{-6}$ m $s^{-1}$ at 0.1 V $s^{-1}$ is not considered. The average deviation between the theoretical and experimental peak-to-peak separations is 0.024 ± 0.014 V. However, when considering only scan rates up to 70 mV $s^{-1}$, this deviation decreases to 0.011 ± 0.004 V. Table 3 shows as well a significant variation of $\Delta E_p$ and $\nu$, confirming that the ferrocyanide couple on SPE is not fully reversible.

This experimental validation section demonstrates that the developed kinetic curves are effective for determining the heterogeneous rate constant $k^0$. Moreover, the derived interpolation equations offer enhanced precision and accuracy in calculating $k^0$ values. These $k^0$ values allowed for the calculation of theoretical CVs that closely match the experimental voltammograms. The experimental validation also highlights that the sum $\alpha + \beta$ should not be systematically assumed to be equal to one, as the determination of $k^0$ highly depends on the values of both anodic and cathodic charge transfer coefficients.

# 5 Conclusions

The soluble–soluble electrochemical system was investigated using the well-known Butler–Volmer equation. Based on a semi-analytical calculation method, cyclic voltammograms were obtained for reversible, quasi-reversible and irreversible redox

systems. Kinetic curves had been established from the peak-to-peak separation criteria, for a wide range of the dimensionless heterogeneous rate constant ($\Lambda$) and the cathodic charge transfer coefficient ($\alpha$). Rational interpolation equations were derived from the kinetic curves. These equations were developed for both cases where $\alpha + \beta = 1$ and where $\alpha + \beta \neq 1$.

Thereafter, an experimental validation involving ferrocyanide redox system was conducted. In this study, the charge transfer coefficients ($\alpha$ and $\beta$), the diffusion coefficient ($D$) and the standard rate constant ($k^0$) were determined. For ferrocyanide ions, the calculated values were $\beta = 0.286 \pm 0.015$, $\alpha = 0.300 \pm 0.016$, $D = (6.43 \pm 0.15) \times 10^{-10}$ m$^2$ s$^{-1}$ and $k^0 = (4.76 \pm 0.49) \times 10^{-6}$ m s$^{-1}$. The average deviation between the theoretical and experimental peak-to-peak separations is 0.024 ± 0.014 V. The theoretical voltammograms simulated using these parameters values closely match with most experimental data points.

Theoretical and experimental results show that when the sum $\alpha + \beta$ is close to 1, the difference between $k^0$ values from the kinetic curves and those from interpolation equations is small. This means that while the kinetic curves give reliable rate constant values, the interpolation equations are more precise. When $\alpha + \beta$ is not close to 1, the kinetic curves are no longer valid, and only the interpolation equations with $\alpha + \beta \neq 1$ could be used.

To the best of our knowledge, this study offers the most thorough investigation into the effects of $\alpha$, $\beta$, and their sum ($\alpha + \beta$) on cyclic voltammetry, with particular emphasis on their impact on peak-to-peak separation and the accurate determination of the heterogeneous rate constant $k^0$. Our findings are supported by detailed simulations and experimental validation, and we critically assess the shortcomings of previously established models. We believe this work provides a significant advancement in electrochemical kinetics, offering a practical and generalizable method for extracting $k^0$ from CV data under a wider range of conditions. As such, it will be of interest to researchers in electrochemistry, physical chemistry, and related disciplines.

## Conflicts of interest

There are no conflicts to declare.

## Data availability

The data supporting this article have been included as part of the supplementary information (SI). Supplementary information: detailed procedures for determining charge transfer and diffusion coefficients of ferrocyanide ions, theoretical validation of interpolation equations, MATLAB code for log(Λ) calculations, a complete nomenclature of symbols and variables, and relevant references. See DOI: https://doi.org/10.1039/d5ra07591b.

## Acknowledgements

The authors acknowledge the financial support offered by the General Direction of Scientific Research and Technology Development, the Algerian Ministry of Higher Education and Scientific Research, Algeria.

## References

1 *Voltammetry: Theory, Types and Applications*, ed. Y. Saito and T. Kikuchi, Nova Publication, New York, 2014.
2 J. E. B. Randles, *Trans. Faraday Soc.*, 1948, **44**, 327–338.
3 A. Ševčík, *Collect. Czech. Chem. Commun.*, 1948, **13**, 349–377.
4 H. Matsuda and Y. Ayabe, *Z. Elektrochem.*, 1955, **59**, 494–503.
5 R. S. Nicholson, *Anal. Chem.*, 1965, **37**, 1351–1355.
6 S. Houam, A. M. Affoune, I. Atek, F. Kesri, R. Saad Guermeche, M. L. Chelaghmia, M. Nacef, O. Khelifi and C. E. Banks, *Electrochim. Acta*, 2023, **449**, 142200.
7 R. S. Nicholson and I. Shain, *Anal. Chem.*, 1964, **36**, 706–723.
8 T. Berzins and P. Delahay, *J. Am. Chem. Soc.*, 1953, **75**, 555–559.
9 G. Mamantov, D. L. Manning and J. M. Dale, *J. Electroanal. Chem.*, 1965, **9**, 253–259.
10 N. White and F. Lawson, *J. Electroanal. Chem. Interfacial Electrochem.*, 1970, **25**, 409–419.
11 D. J. Schiffrin, *J. Electroanal. Chem. Interfacial Electrochem.*, 1986, **201**, 199–203.
12 P. Delahay, *J. Am. Chem. Soc.*, 1953, **75**, 1190–1196.
13 I. Atek, S. Maye, H. H. Girault, A. M. Affoune and P. Peljo, *J. Electroanal. Chem.*, 2018, **818**, 35–43.
14 A. Saila, *Etude des systèmes électrochimiques quasi-réversibles par voltampérométrie à balayage linéaire et semi-intégration : Applications aux comportements de rhénium et dysprosium en milieux de fluorures fondus*, PhD thesis, Université Badji Mokhtar – Annaba, Annaba, 2010.
15 A. M. Affoune, A. Saila, J. Bouteillon and J. C. Poignet, *J. Appl. Electrochem.*, 2006, **37**, 155–160.
16 A. M. Affoune, J. Bouteillon and J. C. Poignet, *J. Appl. Electrochem.*, 2002, **32**, 521–526.
17 A. J. Bard and L. R. Faulkner, *Electrochemical Methods: Fundamentals and Applications*, Wiley, New York, Weinheim, 2nd edn, 2001.
18 J. Heinze, *Angew Chem. Int. Ed. Engl.*, 1993, **32**, 1268–1288.
19 J. Heinze, *Angew Chem. Int. Ed. Engl.*, 1984, **23**, 831–847.
20 S. R. Belding, J. G. Limon-Petersen, E. J. F. Dickinson and R. G. Compton, *Angew. Chem., Int. Ed.*, 2010, **49**, 9242–9245.
21 H. Chen, M. Yang, B. Smetana, V. Novák, V. Matějka and R. G. Compton, *Angew. Chem., Int. Ed.*, 2024, **63**, e202315937.
22 C. K. Terry Weatherly, H. Ren, M. A. Edwards, L. Wang and H. S. White, *J. Am. Chem. Soc.*, 2019, **141**, 18091–18098.
23 E. P. Randviir, *Electrochim. Acta*, 2018, **286**, 179–186.
24 Q. Li, S. Xie, Z. Liang, X. Meng, S. Liu, H. H. Girault and Y. Shao, *Angew. Chem., Int. Ed.*, 2009, **48**, 8010–8013.
25 N. Plumeré and B. A. Johnson, *J. Am. Chem. Soc.*, 2024, **146**, 34771–34785.
26 I. Lavagnini, R. Antiochia and F. Magno, *Electroanalysis*, 2004, **16**, 505–506.
27 J. Heinze and M. Störzbach, *Ber. Bunsenges. Phys. Chem.*, 1986, **90**, 1043–1048.
28 R. J. Klingler and J. K. Kochi, *J. Phys. Chem.*, 1981, **85**, 1731–1741.
29 T. W. Swaddle, *Chem. Rev.*, 2005, **105**, 2573–2608.
30 E. R. Cohen, T. Cvitaš, J. G. Frey, B. Holmström, K. Kuchitsu, R. Marquardt, I. Mills, F. Pavese, M. Quack, J. Stohner,

H. L. Strauss, M. Takami and A. J. Thor, *Quantities, Units and Symbols in Physical Chemistry*, The Royal Society of Chemistry, Cambridge, 3rd edn, 2007.
31 R. G. Compton, E. Laborda and K. R. Ward, *Understanding Voltammetry: Simulation of Electrode Processes*, Imperial College Press, London, 2014.
32 K. B. Oldham and J. Spanier, *J. Electroanal. Chem.*, 1970, **26**, 331–341.
33 K. B. Oldham, *J. Electroanal. Chem. Interfacial Electrochem.*, 1981, **121**, 341–342.
34 H. Chen and R. G. Compton, *J. Electroanal. Chem.*, 2021, **880**, 114942.
35 E. Laborda, M. C. Henstridge, C. Batchelor-McAuley and R. G. Compton, *Chem. Soc. Rev.*, 2013, **42**, 4894.
36 D. Suwatchara, N. V. Rees, M. C. Henstridge, E. Laborda and R. G. Compton, *J. Electroanal. Chem.*, 2012, **665**, 38–44.
37 M. C. Henstridge, E. Laborda, N. V. Rees and R. G. Compton, *Electrochim. Acta*, 2012, **84**, 12–20.
38 I. Kroner, M. Becker and T. Turek, *ChemElectroChem*, 2020, **7**, 4314–4325.
39 M. Becker, N. Bredemeyer, N. Tenhumberg and T. Turek, *Electrochim. Acta*, 2017, **252**, 12–24.
40 G.-S. Tzeng, *Plat. Surf. Finish.*, 1995, **82**, 67–71.
41 E. Agar, C. R. Dennison, K. W. Knehr and E. C. Kumbur, *J. Power Sources*, 2013, **225**, 89–94.
42 S. K. Guin, A. S. Ambolikar and J. V. Kamat, *RSC Adv.*, 2015, **5**, 59437–59446.
43 J. Besson, Précis de thermodynamique et cinétique électrochimiques, in *Handbook of Electrochemical Thermodynamics and Kinetics*, Ellipses-Marketing, Paris, 1984.
44 D. Suwatchara, M. C. Henstridge, N. V. Rees and R. G. Compton, *J. Phys. Chem. C*, 2011, **115**, 14876–14882.
45 M. G. Trachioti, A. Ch. Lazanas and M. I. Prodromidis, *Microchim. Acta*, 2023, **190**, 251.
46 T. Pajkossy, M. U. Ceblin and G. Mészáros, *J. Electroanal. Chem.*, 2021, **899**, 115655.